

Supporting Information

Long-range surface plasmon resonance and surface-enhanced Raman scattering on X-shaped gold plasmonic nanohole arrays

Chao Hou,^{abc} Daniel David Galvan,^a Guowen Meng^c and Qiuming Yu^{*a}

^a Department of Chemical Engineering, University of Washington, Seattle, WA 98195, USA. E-mail: qyu@uw.edu

^b University of Science and Technology of China, Hefei, China.

^c Key Laboratory of Materials Physics, and Anhui Key Laboratory of Nanomaterials and Nanotechnology, Institute of Solid State Physics, Chinese Academy of Sciences, Hefei, 230031, China.

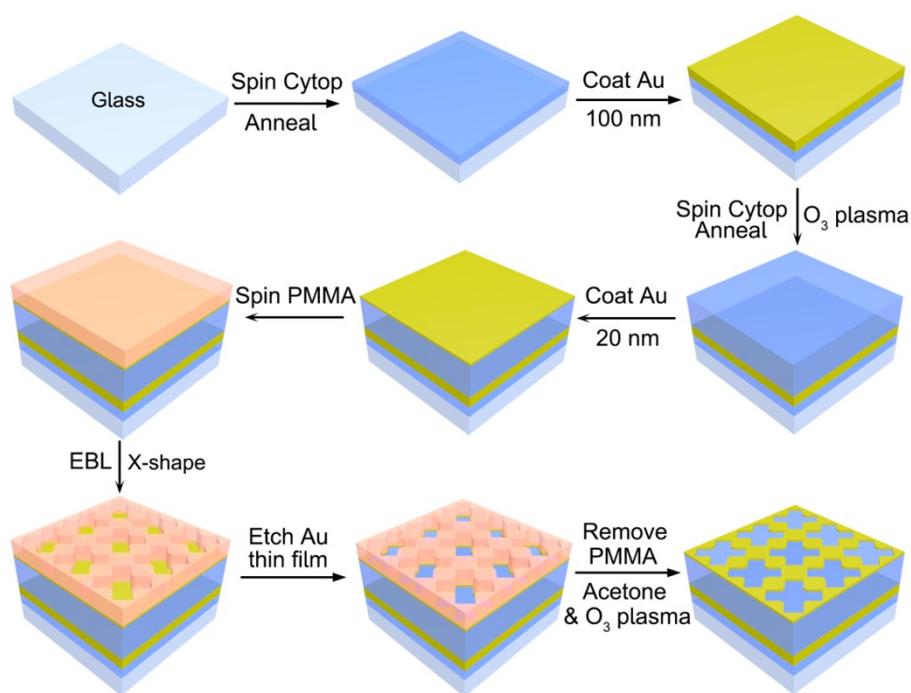


Fig. S1 Schematic for the fabrication of LR-SERS substrates using EBL method. Note that an additional Cytop layer (~100 nm) was added to promote adhesion between the glass substrate and the Au thick film compared to the structure illustrated in Fig. 1.

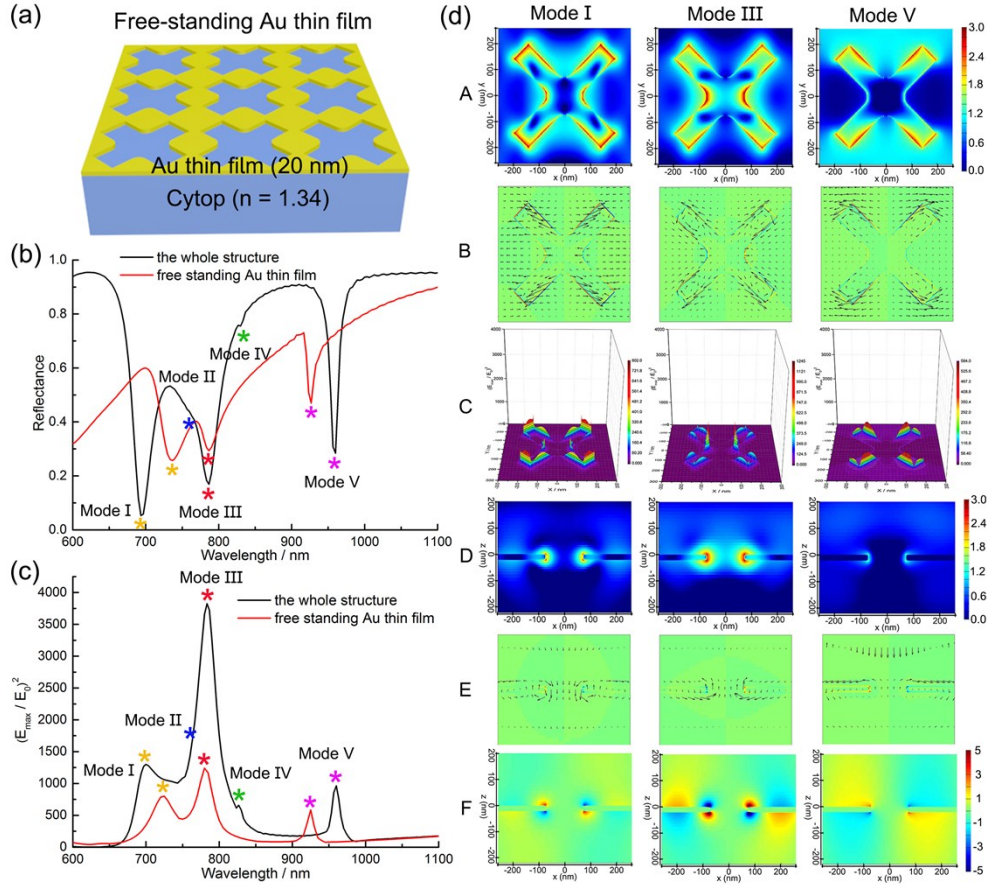


Fig. S2 FDTD simulations of the free-standing substrate without the 100 nm Au thick film (the resonant mirror) but having the Au thin film with 480-80-604 nm (L-W-P) and the Cytop thickness 200 nm. (a) Schematic of the free-standing structure. (b) The reflectance spectra and (c) the electric field enhancement $(E_{\max}/E_0)^2$ versus wavelength. (d) The electric field profiles corresponding to the three resonances of the free-standing structure in (b) and (c). Rows A–C are the distributions at the top Au/water interface while rows D–F are the distributions at the cross-sectional x-z plane. Rows A and D represent $(E_{\max}/E_0)^2$ on a log scale; rows B and E show the maps of the electric charge distribution overlaid with Poynting vectors; row C represents a 3D image of electric field intensity; row F reveals the $|E_z/E_0|$ (E_z is the z-component) on the normal scale.

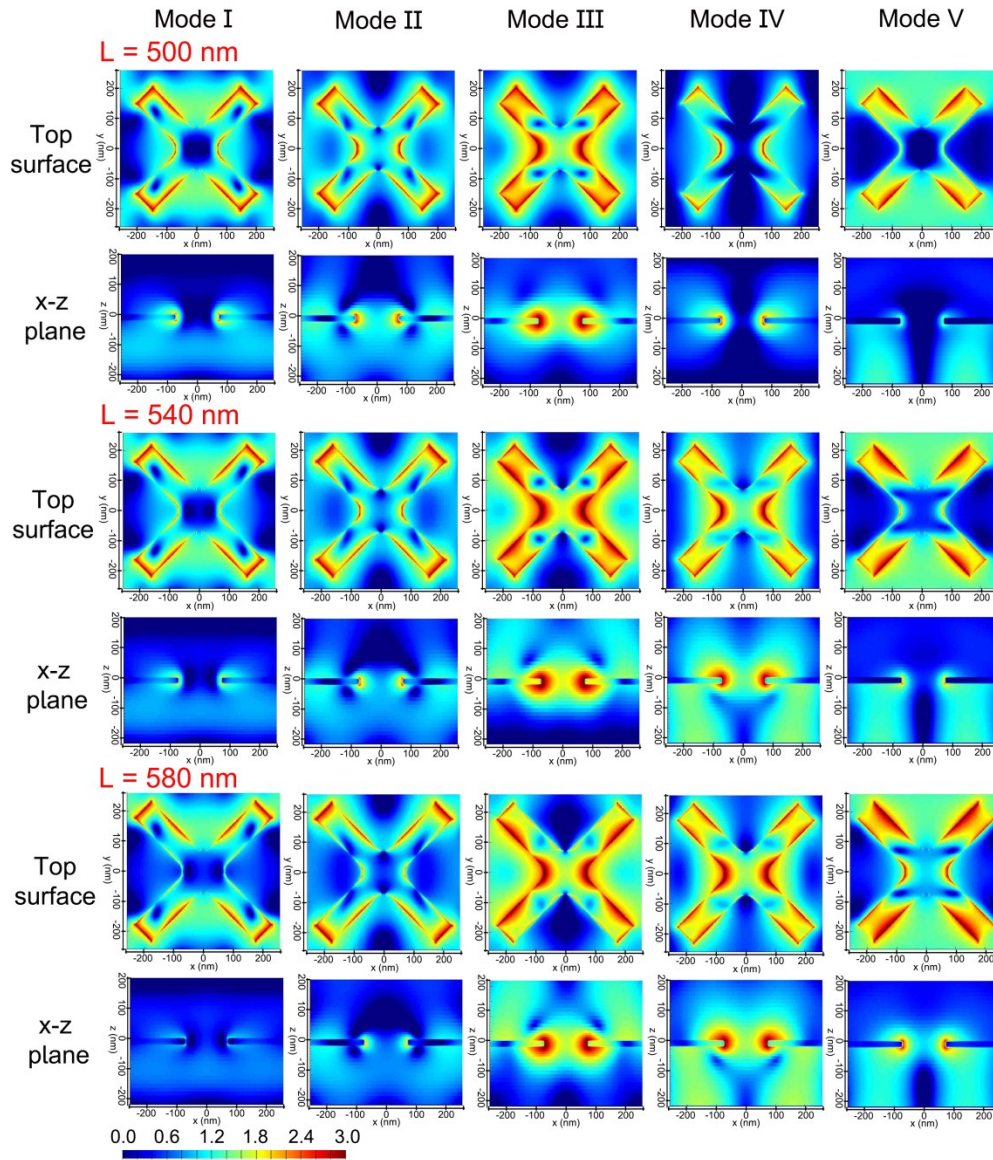


Fig. S3 The FDTD simulated electric field distributions at the top Au/water interface and at the cross-sectional x-z plane for three selected lengths shown in Fig. 4a.

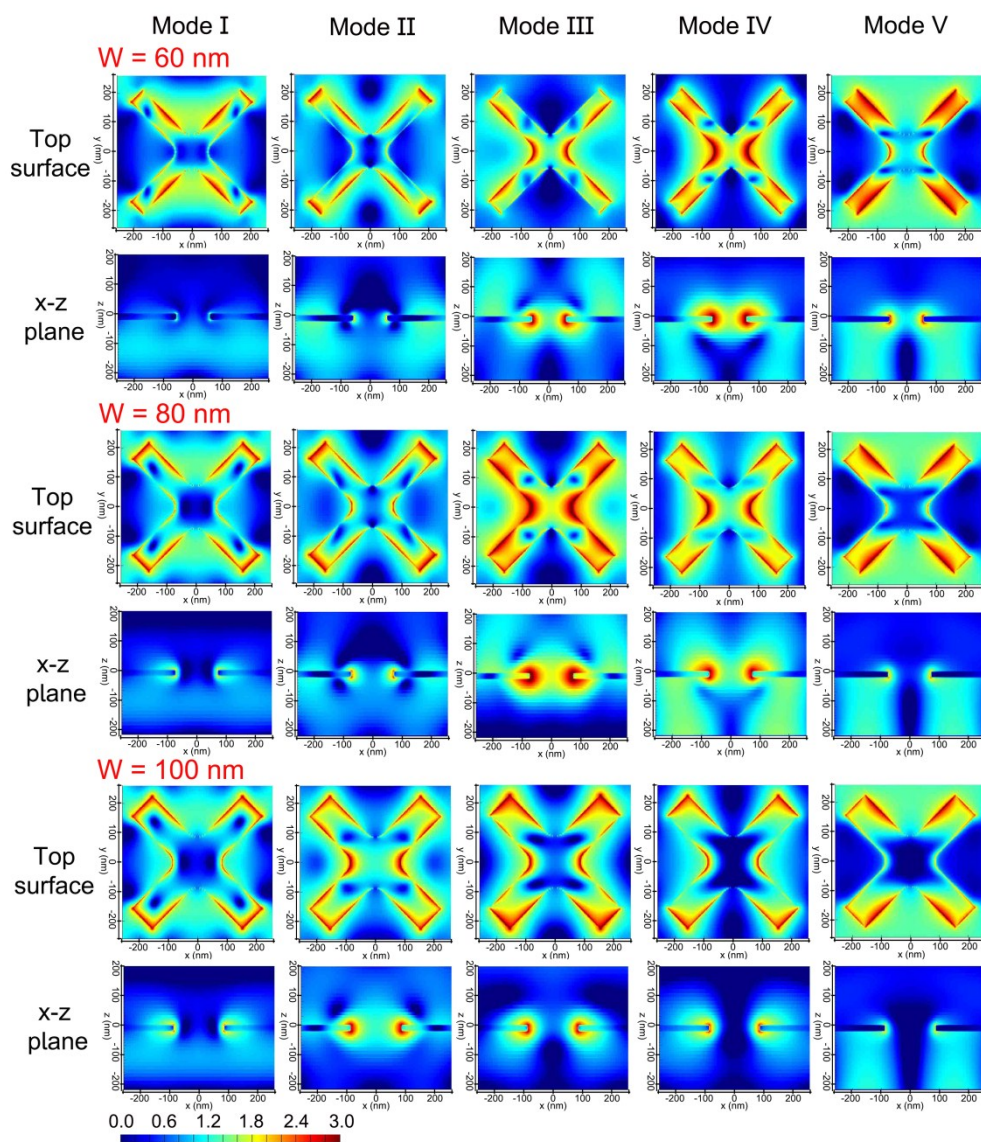


Fig. S4 The FDTD simulated electric field distributions at the top Au/water interface and at the cross-sectional x-z plane for three selected widths shown in Fig. 4b.

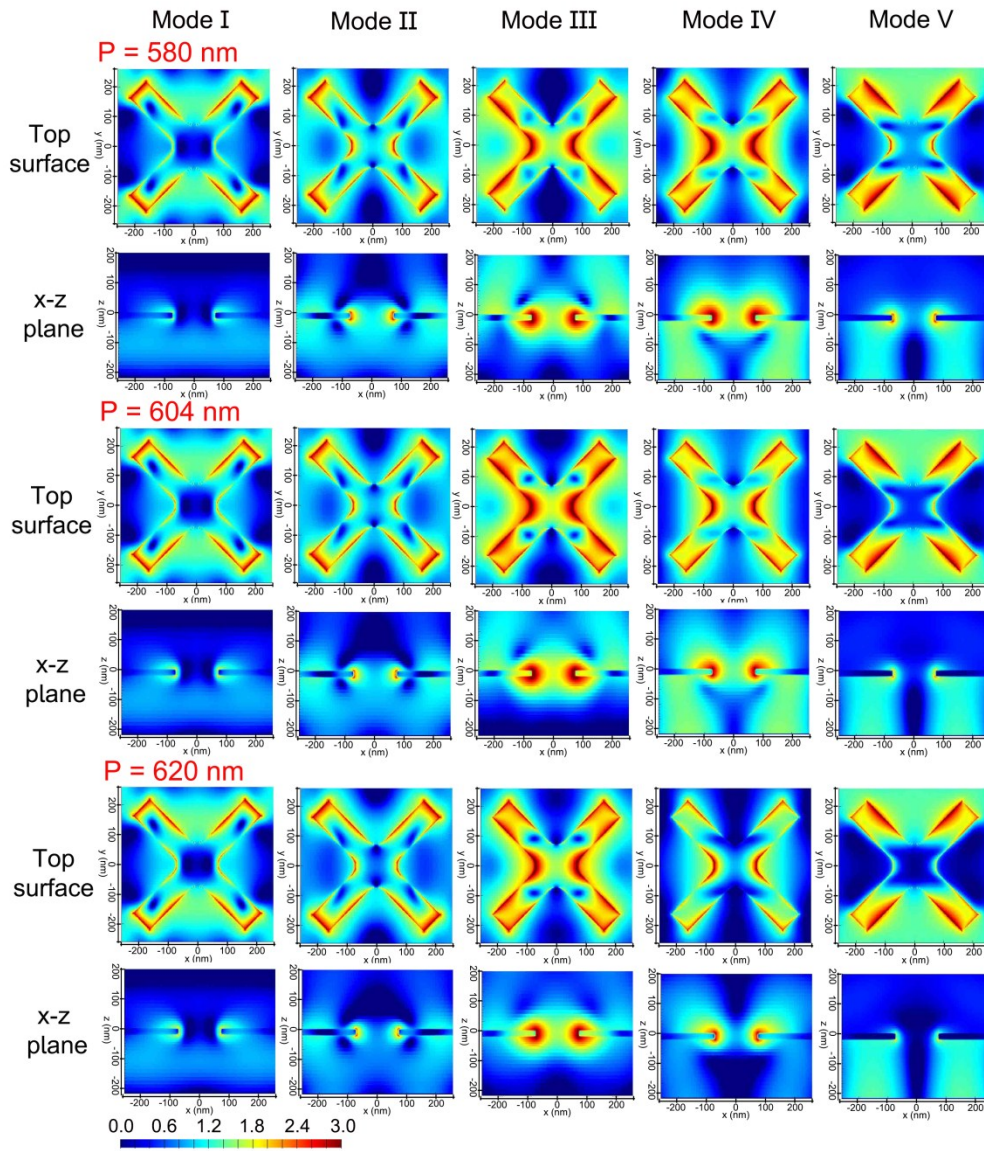


Fig. S5 The FDTD simulated electric field distributions at the top Au/water interface and at the cross-sectional x-z plane for three selected pitches shown in Fig. 4c.

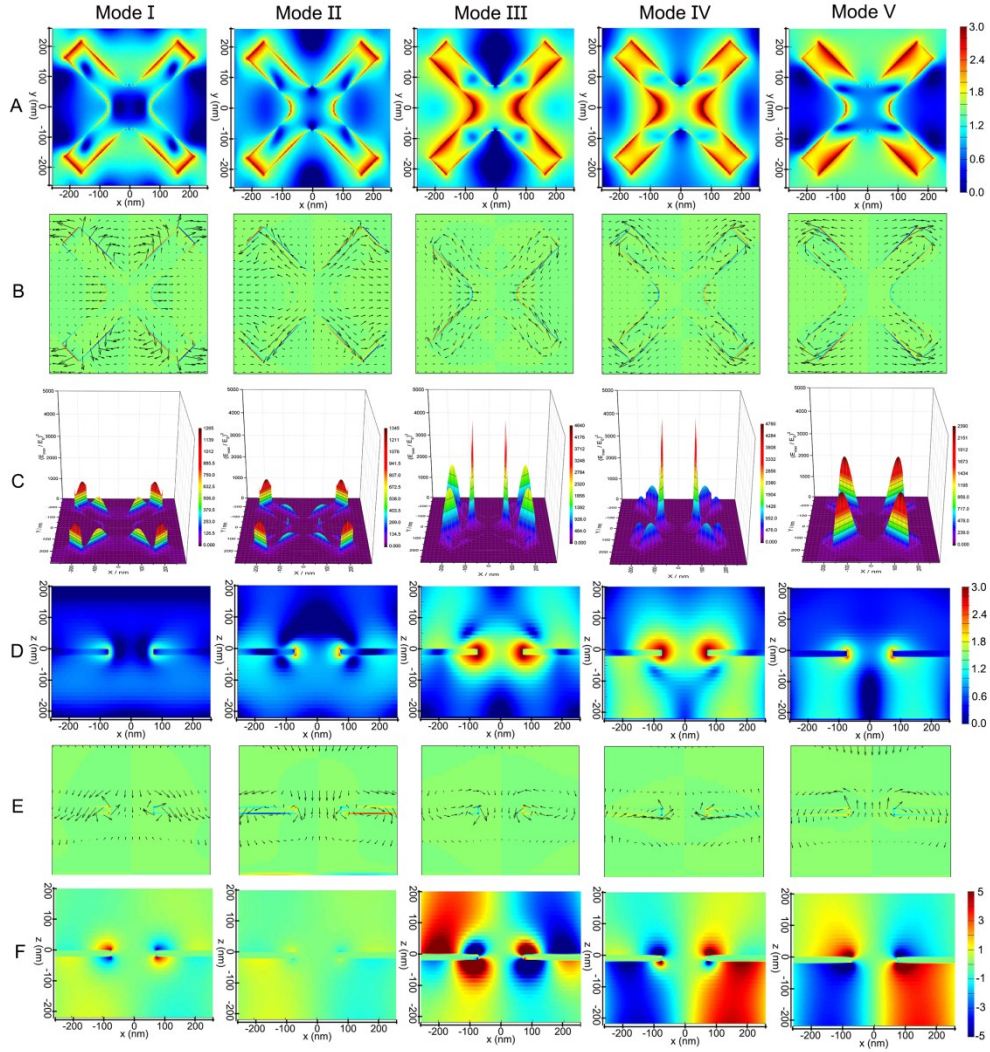


Fig. S6 The electric field profiles and the maps of the electric charge distribution overlaid with Poynting vectors corresponding to all of the five modes for the FDTD simulated optimal conditions 540-80-585-200 nm (L-W-P-T). Rows A–C are the distributions at the top Au/water interface; rows D–F are the distributions at the cross-sectional x-z plane; rows A and D represent $(E_{\max}/E_0)^2$ on a log scale; rows B and E show the maps of the electric charge distribution overlaid with Poynting vectors; row C represents a 3D image; row F reveals the $|E_z/E_0|$ (E_z is the z-component) on the normal scale.